Understanding the Reactivity of Trimethylsilyldiazoalkanes Participating in [3+2] Cycloaddition Reactions towards Diethylfumarate with a Molecular Electron Density Theory Perspective

Luis R. Domingo [1],* , **Nivedita Acharjee [2],*** and **Haydar A. Mohammad-Salim [3]**

[1] Department of Organic Chemistry, University of Valencia, Dr. Moliner 50, Burjassot, E-46100 Valencia, Spain
[2] Department of Chemistry, Durgapur Government College, Durgapur 713214, West Bengal, India
[3] Department of Chemistry, University of Zakho, Duhok 42001, Iraq; hayder.salim@uoz.edu.krd
* Correspondence: domingo@utopia.uv.es (L.R.D.); nivchem@gmail.com (N.A.); Tel.: +91-947-415-0273 (N.A.)

Abstract: A Molecular Electron Density Theory (MEDT) study is presented here for [3+2] cycloaddition (32CA) reactions of three trimethylsilyldiazoalkanes with diethyl fumarate. The presence of silicon bonded to the carbon of these silyldiazoalkanes changes its structure and reactivity from a *pseudomonoradical* to that of a zwitterionic one. A *one-step* mechanism is predicted for these polar *zw-type* 32CA reactions with activation enthalpies in CCl_4 between 8.0 and 19.7 kcal·mol^{-1} at the MPWB1K (PCM)/6-311G(d,p) level of theory. The negative reaction Gibbs energies between −3.1 and −13.2 kcal·mole^{-1} in CCl_4 suggests exergonic character, making the reactions irreversible. Analysis of the sequential changes in the bonding pattern along the reaction paths characterizes these *zw-type* 32CA reactions. The increase in nucleophilic character of the trimethylsilyldiazoalkanes makes these 32CA reactions more polar. Consequently, the activation enthalpies are decreased and the TSs require less energy cost. Non-covalent interactions at the TSs account for the stereoselectivity found in these 32CA reactions involving the bulky trimethylsilyl group.

Keywords: molecular electron density theory; trimethylsilyldiazoalkanes; [3+2] cycloaddition reactions; electron localization function

1. Introduction

Since the last decade, trimethylsilyldiazomethane [1] has been a popular synthetic reagent owing to its commercial availability. This mild, safe, and efficient alternative has been used for the esterification of naturally occurring carboxylic acids [1,2], preparation of silylenol ethers [3], synthesis of gem-silylboronate esters [4], and ring expansion reactions [5], while one of the most important applications of trimethylsilyldiazoalkanes is the generation of functionalized pyrazolines from [3+2] cycloaddition (32CA) reactions with alkene derivatives [6,7] (Scheme 1).
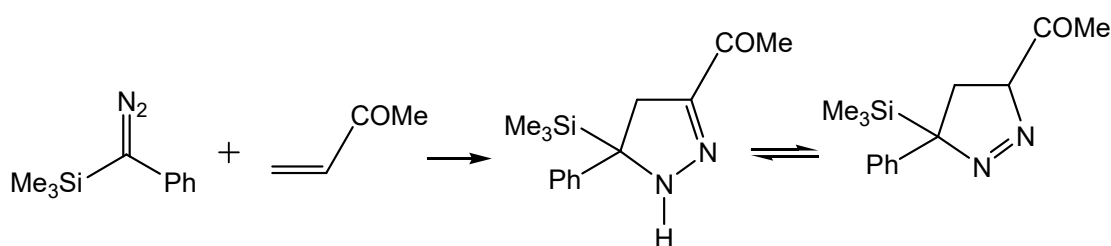

Scheme 1. 32CA reaction of 1-phenyl-1-trimethylsilyldiazomethane and methyl vinyl ketone leading to pyrazoline derivative.

32CA reactions of trimethylsilyldiazoalkanes shelter the unique influence of both steric and electronic effects and have thus invited chemists to explore the mechanism and selectivities over the last four decades. In 1971, Brook and Jones [7] reported 32CA reactions of 1-phenyl-trimethylsilyldiazomethane with methyl vinyl ketone (Scheme 1).

In 1989, Hwu and Wang [8] reviewed the steric influence of trimethylsilyl group in organic synthesis, and subsequently in 1990, Padwa and Wannmaker [9] studied the steric control of trimethylsilyl group on the 32CA reactions of diazoalkanes with trimethylsilyl substituted alkynes.

Whitlock and Carreira [10] performed the enantioselective synthesis of ent-Stellettamide A with antifungal and cytotoxic activities from the 32CA reaction of trimethylsilyldiazomethane (Scheme 2).
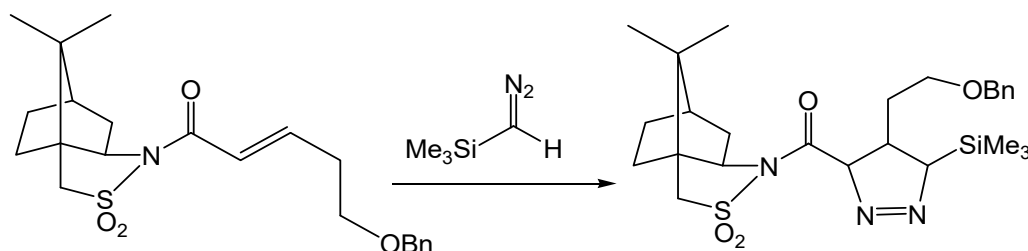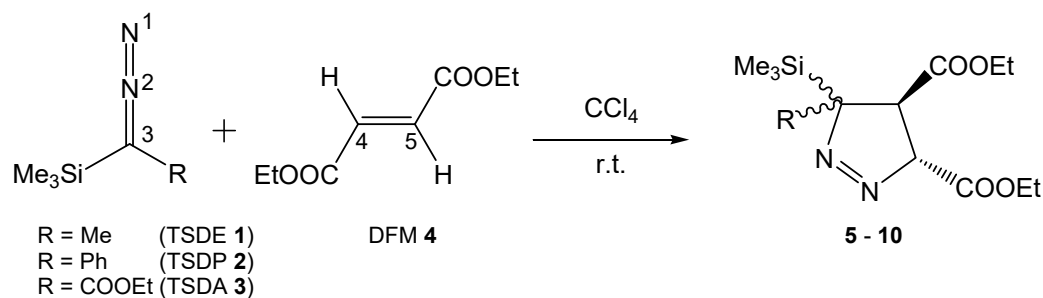

Scheme 2. 32CA reaction of trimethylsilyldiazomethane for synthesis of ent-Stellettamide A.

In 2016, Mlostoń proposed a diradical reaction mechanism for the 32CA reactions of hetaryl thioketones with trimethylsilyl substituted diazomethane [11]. Further, in 2019, he reported the 32CA reactions of trimethylsilyldiazomethane with dicyanofumarate and with dicyanomaleate [12] (see Scheme 3). This reaction proceeds with the elimination of methyl cyanoformate molecule from the cycloadduct and, subsequently, the pyrazole ring system was obtained after aromatization.
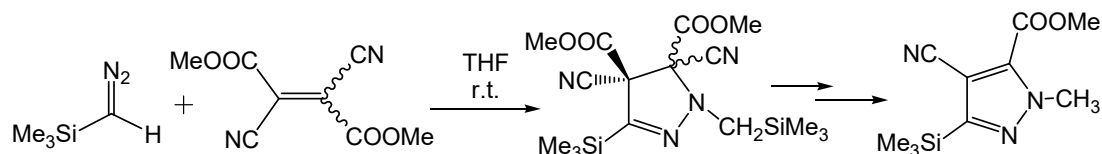
Scheme 3. 32CA reaction of trimethylsilyldiazomethane with dimethylcyanofumarate and dimethylcyanomaleate.

Bassindale and Brook [13] performed the 32CA reactions of 1-trimethylsilyl-1-diazoethane (TSDE) **1**, 1-phenyl-1-trimethylsilyldiazomethane (TSDP) **2** and ethyl-1-trimethylsilyl diazoacetate (TSDA) **3** with diethyl fumarate (DFM) **4** (Scheme 4) to examine the effect of organosilicon substituents on the product composition.

R = Me   (TSDE **1**)
R = Ph   (TSDP **2**)
R = COOEt (TSDA **3**)

Scheme 4. 32CA reaction of trimethylsilyldiazomethane1-trimethylsilyl-1-diazoethane (TSDE) **1**, 1-phenyl-1-trimethylsilyldiazomethane (TSDP) **2**, and ethyl-1-trimethylsilyl diazoacetate (TSDA) **3** with diethyl fumarate DFM **4**.

Experimentally, the relative rates of addition of the diazoalkanes TSDE **1**, TSDP **2**, and TSDA **3** to DFM **4** in carbon tetrachloride (CCl$_4$) at room temperature (Scheme 4) decreases in the order TSDE **1** (1.0) > TSDP **2** (2×10^{-2}) > TSDA **3** ($\approx 2.5 \times 10^{-7}$) [13]. The relative reactivity of silyldiazoalkanes **1**–**3** with DFM **4** was interpreted by Bassindale and Brook [13] from their thermal stability, steric inhibition, and resonance effects, and considering the influence of these effects on the CNDO/2 calculated FMO energies. The low reactivity of TSDA **3** was explained as an outcome of the extraordinary ground state (GS) stability of the CNDO/2 calculated HOMO energy.

With the advent of advanced computations since the last two decades, and the proposal of the pioneering Density Functional Theory (DFT) by Kohn and Sham [14], the use of semi-empirical methods of calculations have been replaced by the DFT calculations and it has been possible to develop new theoretical outlook on organic reactions.

After the proposal of Molecular Electro Density theory [15] (MEDT) by Domingo in 2016, it has been possible to correlate the GS electronic structure of three-atom-components (TACs) and their molecular reactivity [16], which allowed proposing a standard classification [15,16] for the simplest TACs into zwitterionic, carbenoid, *pseudoradical*, and *pseudodiradical*. Interestingly, the reactivity of these TACs in 32CA reactions has put forward a useful classification of the 32CA reactions into zwitterionic type (*zw-type*), carbenoid type (cb-*type*), *pseudo(mono)radical* type (*pmr-type*), and *pseudodiradical* type (*pdr-type*), reactions, with progressive decrease in the activation energies along the series. The *zw-type* reactions are associated with high energy barrier, which is demanding to overcome through sufficient nucleophilic-electrophilic activations [17,18], while the *pdr-type* 32CA reactions show low activation energies and can be performed very easily. This classification has allowed characterizing the simplest diazoalkane as a *pseudoradical* TAC participating in *pmr-type* 32CA reactions (see Figure 1) [19].

pseudoradical structure of diazomethane **11**
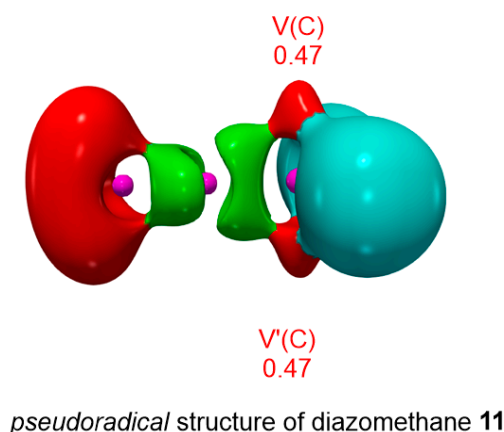
Figure 1. MPWB1K/6-311G(d,p) ELF localization domains (Isosurface value of ELF = 0.75) of the simplest diazomethane **11**. V(C,N) and V(N,N) disynaptic basins are represented in green, V(C,H) disynaptic basin are represented in light blue, V(C) and V(N) monosynaptic basins are represented in red, and C(C) core basins are represented in pink. The valence basin populations of the two V(C) and V'(C) monosynaptic basins are given in average no. of electrons, e.

Herein, an MEDT study for 32CA reactions of silyldiazoalkanes **1**–**3** with DFM **4** (Scheme 4), experimentally reported by Bassindale and Brook, Ref. [13] is carried out in order to understand how the presence of silicon on these silyldiazoalkanes changes the structure and reactivity of these TACs, and thus, explain the experimental outcomes.

We have presented this study into six sections: (1) In Section 3.1, the Electron Localization Function (ELF) topological study [20] at the GS structures of trimethylsilyldiazalkanes **1**–**3** is performed to obtain their respective classification as a TAC [16] and consequently to assess their molecular reactivity in 32CA reactions. (2) In Section 3.2, the Conceptual Density Functional Theory [21,22] (CDFT) indices at the GS of **1**–**4** are analyzed to comprehend the polar character.(3) In Section 3.3, the potential energy surface (PES) along the competitive reaction paths is studied and the energy profiles are analyzed along with

the Global Electron Density Theory [23] (GEDT) calculations at the TSs to confirm the polar character of the reactions. (4) In Section 3.4, a Bonding Evolution Theory [24] (BET) analysis along the 32CA reaction of TSDE **1** and TSDA **3** with DFM **4** is carried out in order to perform a comparative study explaining the relative reactivity of these TACs. (5) In Section 3.5, the ELF of the TSs is studied. Finally, (6) in Section 3.6, the Bader's Quantum Theory of Atoms-in Molecules [25,26] (QTAIM) parameters have been calculated at the reacting sites of the TSs. The Non-Covalent Interactions (NCI) at the TSs is realized through visualization by means of Independent Gradient Model [27] (IGM) analysis based on promolecular density.

2. Computational Methods

The stationary points are optimized at the MPWB1K [28]/6-311G(d,p) [29] level using the Berny analytical gradient optimization method [30]. The use of MPWB1K functional with the 6-311G(d,p) basis set for the analysis of 32CA reactions follows from the single point energy calculations at the CCSD(T)/cc-pVTZ level reported by Domingo in 2018 [17].

Frequency calculations were performed for the optimized geometries to confirm that the transition state structures (TSs) have only one imaginary frequency and that a local minimum has no imaginary frequencies (all positive frequencies). The connection of the corresponding reactants and products via the TSs along the minimum energy reaction pathway was verified through IRC [31] computations using the Gonzales–Schlegel integration method [32,33].

The 32CA reactions were studied using the polarizable continuum model [34,35] (PCM) in the experimental solvent CCl_4. The solvent was modeled using the self-consistent reaction field [36–38] (SCRF) method. The enthalpies, Gibbs free energies, and entropies were calculated in gas phase and toluene with the standard statistical thermodynamics at 298.15 K and 1 atm.

The natural population analysis [39,40] (NPA) was performed at the TSs to obtain the natural atomic charges (q) of the atoms and the summation of these charges at each framework, i.e., the GEDT (f) [23], was computed to determine the direction of the electron density flux at the TSs.

$$\text{GEDT} \ (f) \ = \sum_{q \in f} q$$

Equations reviewed in reference [22] have been used to calculate the CDFT indices [21,22]. All calculations were done using the Gaussian 16 package [41].

Topological analysis of the ELF [20], QTAIM [25,26], and the IGM [27] study was performed using Multiwfn software [42]. IGM isosurfaces were visualized by the VMD [43] program. The Paraview software [44,45] at an isovalue of 0.75 a.u was used to represent the ELF localization domains.

3. Results and Discussion

3.1. ELF Topological Analysis of Trimethylsilyldiazoalkanes TSDE **1**, TSDP **2**, and TSDA **3**, and Diethyl Fumarate DFM **4**

The ELF concept was constructed by Becke and Edgecombe [20] and chemical bonds were subsequently classified by the topological analysis of the ELF by Silvi and Savin [46]. Within the MEDT framework [16], the GS electronic structure of the TACs and their reactivity profile are correlated. Consequently, ELF of trimethylsilyldiazoalkanes **1**–**3** have been studied to analyze their reactivity in 32CA reactions. Table 1 lists the significant valence basin populations. The ELF localization domains, the proposed ELF-based Lewis-like structures, and the natural atomic charges of TSDE **1**, TSDP **2**, TSDA **3**, and DFM **4** are given in Figure 2, while a representation of ELF localization domains of TSDE **1** is shown in Figure 3.

Table 1. The Electron Localization Function (ELF) valence basin populations (in average number of electrons, e) at the GS structures of the reagents **1–4**, calculated using MPWB1K functional with the 6-311G(d,p) basis set.

	1	2	3	4
V(N1)	3.82	3.74	3.63	
V(N1,N2)	1.79	1.81	1.89	
V'(N1,N2)	1.90	1.91	1.97	
V(C3,N2)	3.07	3.06	2.93	
V(C3,C6)	1.87	2.17	2.36	
V(C3,Si)	3.19	3.07	3.11	
V(C4,C5)				1.67
V'(C4,C5)				1.65
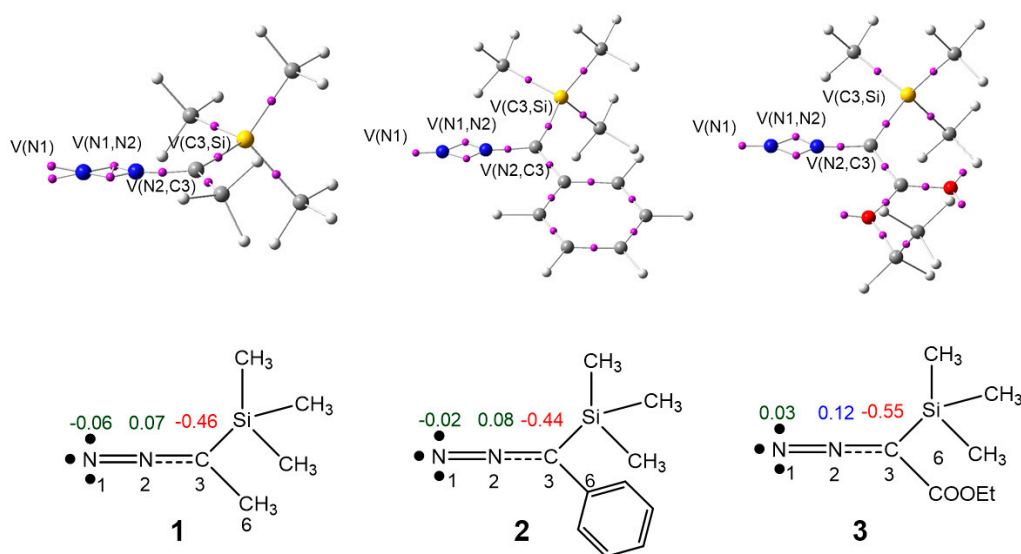
Figure 2. MPWB1K/6-311G(d,p) ELF basin attractor positions, ELF-based Lewis-like structures, and natural atomic charges, in average number of electrons e, of TSDE **1**, TSDP **2**, and TSDA **3**. Red, green, and blue colors are used to show the negative, negligible, and positive charges, respectively.
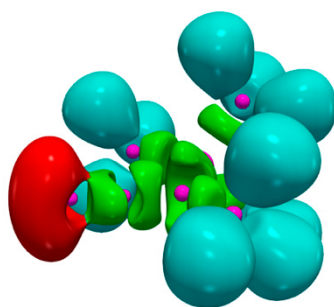
Figure 3. ELF localization domains (isosurface value = 0.75) of TSDE **1**. Blue color is used to show protonated basins, red color for the monosynaptic basins, green color for the disynaptic basins, and magenta color for core basins. Calculations are done at MPWB1K/6-311G(d,p) level.

The electronic structure at the N1-N2-C3 moiety of silyldiazoalkanes TSDE **1**, TSDP **2,** and TSDA **3** is presented from the total integrating basin populations at the attractor positions. The V(N1) monosynaptic basin is associated with the N1 nitrogen lone pair, integrating 3.82 e (**1**), 3.74 e (**2**), and 3.63 e (**3**). It is interesting to note from Figure 2 that the ELF of TSDE **1** shows two attractors associated with the monosynaptic basin V(N1), while a single attractor corresponding to the V(N1)

monosynaptic basin is shown for TSDP **2** and TSDA **3**, suggesting the influence of substituent effects on the electronic framework of the trimethylsilyldiazoalkanes.

The C3-N2 and N1-N2 double bonds are underpopulated, respectively, being associated with the V(C3,N2) disynaptic basin, integrating 3.07 e (**1**), 3.06 e (**2**), and 2.93 e (**3**) and V(N1,N2) and V'(N1,N2) disynaptic basins integrating 3.69 e (**1**), 3.72 e (**2**), and 3.86 e (**3**).

ELF topology of these silyldiazoalkanes shows also the presence of one V(C3,C6) disynaptic basin, integrating 1.87 e (**1**), 2.17 e (**2**), and 2.36 e (**3**), associated with the underpopulated C3-C6 single bond, and one V(C3,Si) disynaptic basin, integrating 3.19 e (**1**), 3.07 e (**2**) and 3.11 e (**3**), associated with the overpopulated C3-Si single bond. The high populations of the V(C3,Si) disynaptic basins result from the delocalisation of the electron density of the *pseudoradical* V(C3) monosynaptic basin present in the simplest diazomethane **11** (see Figure 1) into the neighbouring silicon center. This behaviour accounts for the change of the *pseudo(mono)radical* structure of the simplest diazomethane **11** to the zwitterionic one of silyldiazoalkanes **1**–**3**.

The C4-C5 double bond in DFM **4** is underpopulated, being associated with the V(C4,C5) and V'(C4,C5) disynaptic basins with the total integrating population 3.32 e.

The natural atomic charges at N1, N2 and C3 are given in Figure 2. N1 and N2 nitrogens show negligible charges, while the C3 carbon is negatively charged with values −0.46 e (**1**), −0.44 e (**2**) and −0.55 e (**3**). Thus, the computed charges rule out the conventional zwitterionic Lewis electronic structure of the diazoalkanes. Note that the zwitterionic classification [16] used herein for the TACs **1**–**3** does not consider charges, instead the specific bonding pattern is taken into account.

3.2. Analysis of the CDFT Indices of the Reactants

The reactivity of TACs and ethylenes participating in 32CA reactions [16] can be successfully comprehended from the analysis of CDFT indices [21,22]. The B3LYP/6-31G(d) computational level is employed for CDFT analysis to assess the reactivities in accordance to the standard electrophilicity [47] and nucleophilicity scales (see Table 2) [48].

Table 2. Conceptual Density Functional Theory (CDFT) indices of TSDE **1**, TSDP **2**, TSDA **3**, and DFM **4** calculated at the B3LYP/6-31G(d) level. The electronic chemical potential and chemical hardness are denoted by μ and η while the electrophilicity and nucleophilicity indices are denoted by ω and N, respectively. All values are represented in eV.

	μ	η	ω	N
1	−3.12	4.60	1.06	3.70
2	−3.22	4.11	1.27	3.84
3	−3.89	4.84	1.56	2.80
4	−4.84	5.39	2.18	1.58

The electronic chemical potentials [49] μ of these silyldiazoalkanes, $\mu = -3.12$ eV (**1**), −3.22 eV (**2**), and −3.89 eV (**3**), are higher than that of DFM **4**, $\mu = -4.84$ eV, suggesting that along a polar 32CA reaction, the electron density will flux from these silyldiazoalkanes to DFM **4**.

The silyldiazoalkanes TSDE **1** and TSDP **2** are classified as moderate electrophiles [47,50] with $\omega = 1.06$ (**1**) and 1.27 eV (**2**) and TSDE **3** as a strong electrophile with $\omega = 1.56$ eV. On the standard nucleophilicity scale [48], TSDE **1** and TSDP **2** show values higher than 3.00 eV (N= 3.70 (**1**) and 3.84 (**2**) eV) and are classified as strong nucleophiles [51], while TSDA **3**, N= 2.80 eV is classified as a moderate nucleophile. Thus, increase in electrophilicity is observed due to the presence of carbethoxy substituent in TSDA **3**, relative to the presence of methyl and phenyl substituents in TSDE **1** and TSDP **2**.

DFM **4** is classified as a strong electrophile with electrophilicity index $\omega = 2.18$ eV and as a weak nucleophile with nucleophilicity index $N = 1.58$ eV.

Consequently, along these 32CA reaction, DFM **4** will behave as a strong electrophile while silyldiazoalkanes **1–3** will behave as nucleophiles, in clear agreement with the electronic chemical potentials of these species.

3.3. Analysis of the Energy Profile of the Stationary Points along the Feasible Reaction Paths for 32CA Reactions of TSDE 1, TSDP 2, and TSDA 3, with DFM 4

Due to the molecular symmetry of DFM **4**, the regiochemical preference is not feasible for these 32CA reactions. On the other hand, due to the non-symmetry of these silyldiazoalkanes, two stereoisomeric reaction paths are feasible depending on the approach mode of the bulky trimethylsilyl group with respect to the carboxylate group present at the C4 carbon of DFM **4**. Along the two feasible stereoisomeric reaction paths, the reactants, TSDE **1**, TSDP **2**, TSDA **3**, and DFM **4**, TSs, **TS1**, **TS2**, **TS3**, **TS4**, **TS5**, and **TS6**, and the corresponding pyrazolines, **5–10**, were located and characterized for the 32CA reactions (Scheme 5). At **TS1**, **TS3**, and **TS5**, the bulky trimethylsilyl group is located over the C4 carboxylate group, while at **TS2**, **TS4**, and **TS6** it is far. The relative energies, enthalpies, entropies, and free energies of the TSs and the cycloadducts are listed in Table 3.
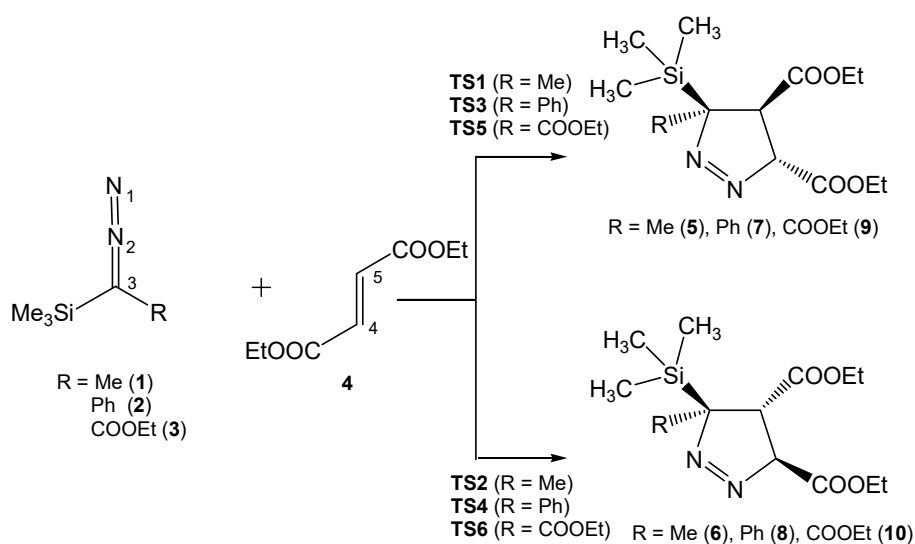
Scheme 5. Studied reaction paths of 32CA reactions of TSDE **1**, TSDP **2**, and TSDA **3** with DFM **4**.

Table 3. MPWB1K/6-311G(d,p) relative energies ΔE in kcal·mol^{-1}, enthalpies, ΔH in kcal·mol^{-1}, entropies, ΔS in cal·mol^{-1}·K^{-1}, and Gibbs free energies, ΔG in kcal·mol^{-1}, computed at 298.15 K and 1 atm in gas phase and in CCl$_4$, of the TSs and products of 32CA reactions of TSDE **1**, TSDP **2**, and TSDA **3**, with DFM **4**. The Global Electron Density Theory (GEDT) is given in e.

	Gas Phase					**CCl$_4$**				
	ΔE	**ΔH**	**ΔS**	**ΔG**	**GEDT**	**ΔE**	**ΔH**	**ΔS**	**ΔG**	**GEDT**
TS1	9.4	10.4	−58.6	27.9	0.27	9.7	10.3	−55.5	26.8	0.28
5	−32.4	−29.4	−61.3	−11.2		−32.5	−29.4	−61.8	−11.0	
TS2	7.6	8.1	−56.1	24.9	0.26	7.6	8.0	−55.7	24.6	0.27
6	−32.3	−29.5	−54.7	−13.3		−32.4	−29.7	−55.1	−13.2	
TS3	14.0	14.4	−52.1	29.9	0.23	14.5	14.7	−52.5	30.4	0.24
7	−28.0	−25.9	−59.2	−8.2		−27.4	−25.4	−58.6	−8.0	
TS4	11.3	10.8	−53.4	26.7	0.21	11.6	11.8	−53.6	27.8	0.22
8	−25.8	−24.6	−62.8	−5.9		−25.7	−24.5	−63.1	−5.7	
TS5	18.6	19.0	−51.8	34.4	0.19	19.3	19.7	−50.8	34.9	0.20
9	−20.3	−17.7	−49.6	−2.9		−20.5	−17.9	−49.9	−3.1	
TS6	15.6	15.2	−54.5	31.4	0.19	16.4	16.5	−51.0	31.7	0.20
10	−21.4	−19.6	−54.0	−3.5		−21.6	−19.8	−55.1	−3.3	

These 32CA reactions show activation enthalpies between 8.1 (**TS2**) and 19.0 (**TS5**) kcal·mol^{-1} in gas phase, and between 8.0 (**TS2**) and 19.7 (**TS5**) kcal·mol^{-1} in CCl$_4$ at 298 K (see Table 3). The exergonic character is evident from the reaction Gibbs free energies between −13.3 (**6**) and −2.9 (**9**) kcal·mol^{-1} in gas phase, and between −13.2 (**6**) and −3.1 (**9**) kcal·mol^{-1} in CCl$_4$ (see Table 3).

The studied energy profile allows arriving at some important conclusions: (i) Consideration of solvent effects in CCl$_4$ shows minimal changes in the activation and reaction enthalpies within 1 kcal·mol^{-1}, this difference being slightly higher to 1.3 kcal·mol^{-1} for **TS6**; (ii) the activation enthalpy of 32CA reaction of TSDE **1** with DFM **4** is lower than that of the 32CA reactions of TSDP **2** and TSDA **3** with DFM **4** by 3.8 (2.7 kcal·mol^{-1} in gas phase) and 8.5 (7.1 kcal·mol^{-1} in gas phase) in CCl$_4$, respectively, at 298 K. This agrees well with the experiments, in which the 32CA reaction of TSDP **2** with DFM **4** is 2×10^{-2} times slower than that of TSDE **1** with DFM **4,** while the 32CA reaction of TSDA **3** with DFM **4** is 2.5×10^{-7} times slower than that of TSDE **1** with DFM **4** (see Scheme 4); [12]. (iii) For each 32CA reaction, the approach of the bulky trimethylsilyl group in TSDE **1**, TSDP **2**, and TSDA **3** avoids steric interaction with the COOEt substituent of DFM **4** in the favored TS, evident from the lowering of the activation enthalpy of **TS2** by 2.3 kcal·mol^{-1} (2.3 kcal·mol^{-1} in gas phase) relative to **TS1**, that of **TS3** lowered by 2.9 kcal·mol^{-1} (3.6 kcal·mol^{-1} in gas phase) relative to **TS4**, and that of **TS6** lowered by 3.2 kcal·mol^{-1} (3.8 kcal·mol^{-1} in gas phase) relative to **TS5**; (iv) the negative Gibbs free energies of these 32CA reactions suggests exergonic character, which makes them irreversible; and finally, (v) The activation Gibbs free energies are increased by between 15.4 and 17.5 kcal·mol^{-1} in gas phase and between 15.2 and 16.6 kcal·mol^{-1} in CCl$_4$ relative to the activation enthalpies, owing to the entropy consideration of these bimolecular reactions. The exergonic character of these 32CA reactions are decreased between 14.8 and 18.7 kcal·mol^{-1} in gas phase and between 14.8 and 18.8 kcal·mol^{-1} in CCl$_4$.

The gas phase optimized geometries of the TSs are given in Figure 4. These TSs geometries show minimal changes on inclusion of solvent effects in CCl$_4$. The distances between C3 and C4, and between N1 and C5 in the TSs, are higher than 2.0 Å. The formation of C-C and C-N bonds start at 2.0–1.9 and 1.9–1.8 Å, respectively [16]. Consequently, these 32CA reactions involve early TSs in which the C-C and C-N bond formation has not yet been started.

Finally, the GEDT [23] at the TSs are calculated and analyzed to predict the polar character of these 32CA reactions. The computed GEDT at gas phase optimized TSs are 0.27 e at **TS1**, 0.26 e at **TS2**, 0.23 e at **TS3**, 0.21 e at **TS4**, 0.19 e at **TS5**, and 0.19 e at **TS6** (see Table 3), suggesting polar processes characterized by GEDT values above 0.20 e. In CCl$_4$, the GEDT values at the TSs do not show any substantial change (see Table 3). The predicted polar character of these *zw-type* 32CA reactions agrees with the CDFT analysis at the GS of the reagents (Table 2).

Note that the polarity decreases progressively when the methyl substituent of TSDE **1** is replaced by phenyl in TSDP **2** and with carbethoxy group in TSDA **3**, attributed to the decrease in the nucleophilicity from TSDE **1** to TSDA **3** (Table 2), resulting in less reaction polarity with highly electrophilic DFM **4**.
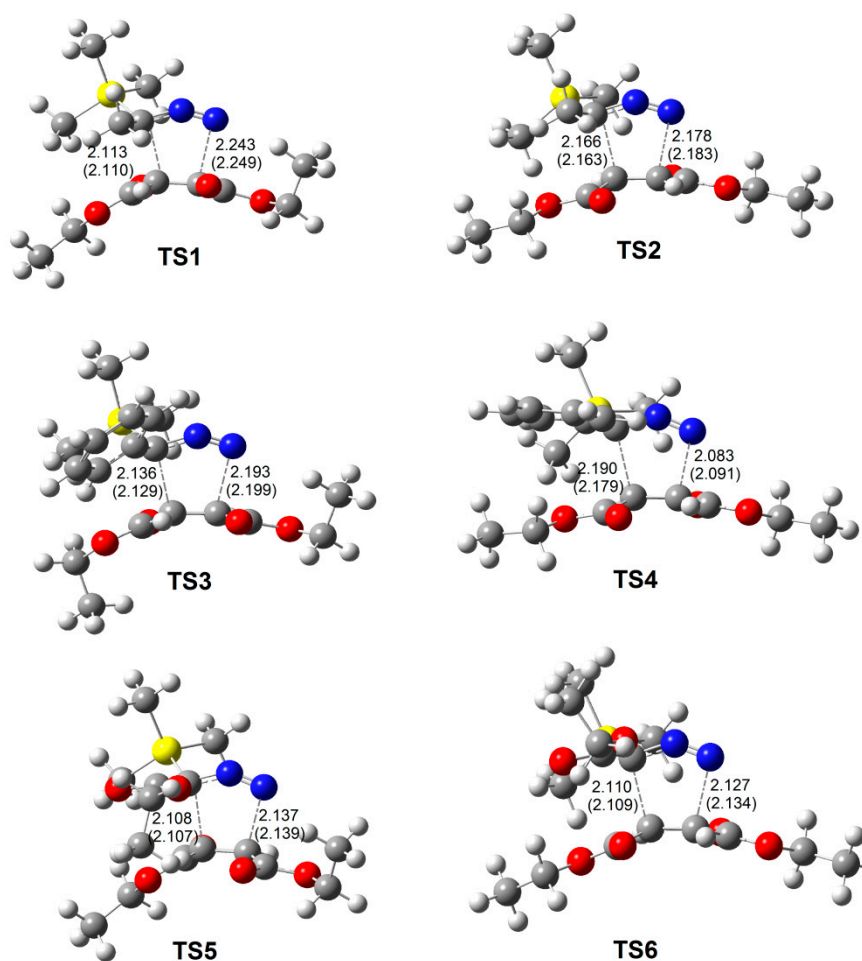
Figure 4. Gas phase optimized geometries of TSs involved in the 32CA reactions of TSDE **1**, TSDP **2**, and TSDA **3**, with diethyl fumarate (DFM) **4**. Bond lengths are expressed in Angstrom unit. Bond lengths calculated in CCl$_4$ are given in parenthesis.

3.4. BET Study of the 32CA Reaction of TSDE **1** and TSDA **3** with DFM **4**

The sequential changes in the bonding pattern along the 32CA reactions of DFM **4** with TSDE **1** and with TSDA **3** have been characterized and compared by BET [24] study; the details are given in Sections 1 and 2 in Supplementary Materials.

The BET study of the 32CA reactions of DFM **4** with TSDE **1** allows arriving at some important conclusions: (i) Identification of the catastrophes along this reaction path divides the 32CA reaction into nine different *phases*. (ii) From **S1-I** to **S4-I**, the C3-N2 bonding region of TSDE **1** is depopulated to create the N2 lone pair and *pseudoradical* centre at C3, while at **S5-I**, the C4-C5 bonding region of DFM **4** is depopulated to create *pseudoradical* centre at C4. From **S1-I** to **S5-I**, the energy cost (EC) is 7.6 kcal·mol^{-1}, equal to the activation energy of **TS2**. (iii) *Phase VII* begins at **S7-I**, identified by the formation of the disynaptic V(C3,C4) basin (see Figure 5) integrating 1.26 e. At this IRC point, the formation of first C3-C4 single bond at the C-C distance of 1.96 Å begins by the coupling of C3 and C4 *pseudoradicals*. The V(C5) monosynaptic basins created in *Phase VI*, which is demanded for the subsequent N1-C5 single bond formation, has reached a populations of 0.33 e. (iv) *Phase IX* begins at **S9-I**, identified by the formation of disynaptic V(N1,C5) basin (see Figure 5) integrating 1.32 e. At this IRC point, the formation of second N1-C5 single bond at the N-C distance of 1.77 Å begins by the coupling of the *pseudoradical* centre at C5 carbon and the non-bonding electron density at N1 nitrogen.
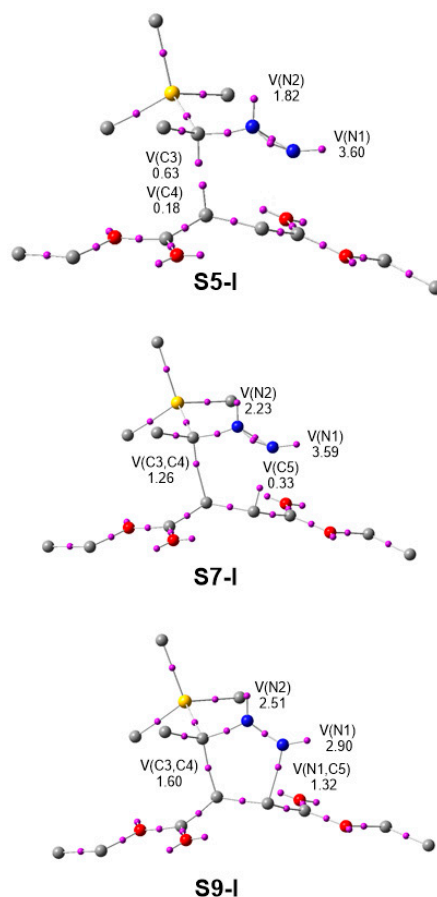
Figure 5. ELF basin attractor positions at the IRC structures **S5-I**, **S7-I**, and **S9-I** along the 32CA reaction of TSDE **1** with DFM **4**.

BET study of the 32CA reactions of DFM **4** with TSDA **3** allowed arriving at some important conclusions: (i) Identification of the catastrophes along this reaction path divides the 32CA reaction into nine different *phases*. (ii) From **S1-II** to **S4-II**, the C3-N2 bonding region of TSDA **3** is depopulated to create the N2 lone pair and *pseudoradical* centre at C3, while at **S5-II**, the C4-C5 bonding region of DFM **4** is depopulated to create *pseudoradical* centre at C4. From **S1-II** to **S5-II**, the EC is 15.5 kcal·mol^{-1}, equal to the 99% of the activation energy of **TS6**. (iii) *Phase VII* begins at **S7-II**, identified by creation of the disynaptic V(C3,C4) basin integrating 1.10 e. At this IRC point, the formation of first C3-C4 single bond at the C-C distance of 2.00 Å begins by the coupling of C3 and C4 *pseudoradicals*. (iv) *Phase IX* begins at **S9-II**, identified by the formation of disynaptic V(N1,C5) basin integrating 1.30 e. At this IRC point, the formation of second N1-C5 single bond at the N-C distance of 1.74 Å begins by the coupling of the *pseudoradical* centre at C5 carbon and the non-bonding electron density at N1 nitrogen.

The comparative BET study of the 32CA reactions of DFM **4** with TSDA **1** and with TSDA **3** allows arriving at some important conclusions: (i) These two 32CA reactions show considerable similitude in the sequential changes of the bonding pattern along the reaction path. The EC demanded to reach the IRC point **S5-I**, which corresponds to 100% of the activation energy of the 32CA reaction of DFM **4** with TSDA **1**, is 7.9 kcal·mol^{-1} lower than that required to reach the IRC point **S5-II**, which corresponds to 99.9% of the activation energy of the 32CA reaction of DFM **4** with TSDA **3**. Note that primarily, the C3-N2 and C4-C5 bonding regions are depopulated along the reaction path to reach the activation energies. The difference in activation energy of the two reactions suggests that the observed acceleration in the 32CA reaction of TSDE **1** is the outcome of the feasible depopulation of the C4-C5 bonding region in DFM **4** relative to that in the 32CA reaction of TSDA **3**.

The GEDT at **S5-I** is 0.26 e and at **S5-II** is 0.19 e, suggesting the role of increased GEDT to lower the EC; as a result, the olefinic double bond in DFM **4** is easily depopulated in these polar 32CA reactions [52]. It is also interesting to note that the merging of two V(C4,C5) disynaptic basins into one V(C4,C5) for the 32CA reaction of TSDE **1** with DFM **4** at **S2-I** requires EC of 2.4 kcal·mol^{-1}, while the similar change in bonding pattern for the 32CA reaction of TSDA **3** with DFM **4** at **S2-II** is 9.4 kcal·mol^{-1}; (ii) the present MEDT study suggests that the C4-C5 double bond of DFM **4** is easily depopulated to create the two *pseudoradicals* due to increased GEDT along the polar 32CA reaction of TSDE **1** with DFM **4** compared to that of the 32CA reaction of TSDA **3** with DFM **4** [52].

3.5. ELF Topological Analysis at the TSs

The ELF valence populations at the TSs are given in Table 4 while the basin attractor positions at the more favorable stereoisomeric TSs are shown in Figure 6. A great similitude is observed in the geometrical aspects of the TSs (see Figure 4).

Table 4. The ELF valence basin populations (in average number of electrons, e) of the TSs, calculated using MPWB1K functional with the 6-311G(d,p) basis set.

	TS1	**TS2**	**TS3**	**TS4**	**TS5**	**TS6**
V(N1)	3.57	3.60	3.57	3.59	3.52	3.52
V(N1,N2)	1.53	1.44	1.44	1.31	1.55	1.55
V'(N1,N2)	1.63	1.67	1.69	1.72	1.56	1.55
V(N2)	1.76	1.82	1.82	1.94	1.85	1.88
V(C3,N2)	2.07	2.07	2.05	2.05	2.05	2.03
V(C3,C6)	1.91	1.92	2.13	2.19	2.41	2.30
V(C3,Si)	2.27	2.28	2.25	2.28	2.31	2.29
V(C4,C5)	2.94	2.96	2.95	2.93	2.91	2.91
V(C3)	0.67	0.63	0.62	0.55	0.62	0.62
V(C4)	0.23	0.18	0.19	0.20	0.23	0.20
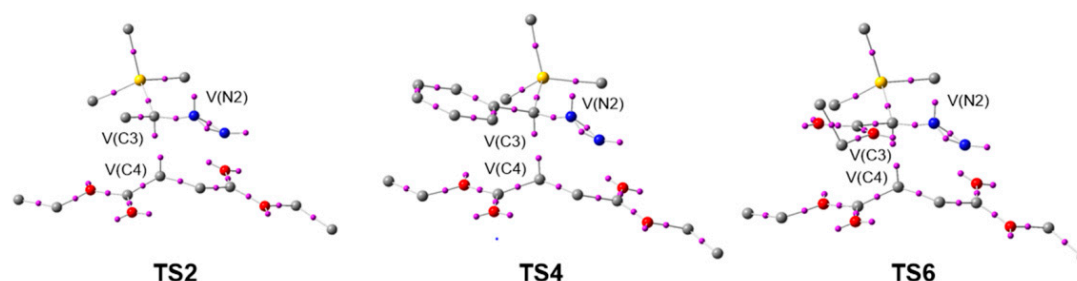
Figure 6. ELF basin attractor positions of **TS2**, **TS4**, and **TS6**.

At the six TSs, the formation of the two *pseudoradicals* C3 and C4 carbons are observed, which are not present in either TSDE **1**, TSDP **2**, and TSDA **3** nor DFM **4**. The two monosynaptic basins V(C3) and V(C4) associated with these *pseudoradicals* show the total integrating populations between 0.55 and 0.67 e and between 0.18 and 0.23 e, respectively. The C3-N2 and C4-C5 bonding regions at the TSs show depopulation relative to that in the reagents, which is demanded to create the *pseudoradicals* at C3 and C4 carbons. Note that the disynaptic V(C3,N2) basin integrating 3.07 e in TSDE **1** is depopulated to 2.07 e in **TS1** and **TS2**, integrating 3.06 e in TSDP **2** is depopulated to 2.05 e in **TS3** and **TS4**, and integrating 2.93 e in TSDP **3** is depopulated to 2.05 e in **TS5** and to 2.03 in **TS6**. The C4-C5 bonding region in DFM **4** integrating 3.32 e is depopulated between 2.91 and 2.96 e at the TSs.

At the TSs, the formation of disynaptic V(C3,C4) and V(N1, C5) is not observed, suggesting that the formation of new single bonds occurs at the later phases along the reaction path and not at the TSs. This is in agreement with the optimized TS geometries showing the C-C and N-C forming bond lengths

above 2.0 Å (Figure 4) and is also in conformity with the topological analysis of the AIM discussed in Section 3.6.

3.6. QTAIM and IGM Topological Analysis at TSs

The topological analysis of the AIM proposed by Bader and coworkers [25,26] was carried out to predict the nature of interatomic interactions at the TSs. The calculated QTAIM parameters, the electron density ρ, Laplacian of electron density $\nabla^2\rho(r_c)$, and energy density $E_{\rho(r_c)}$ in au, at the bond critical points (3,−1) at the TSs, are given in Table 5.

Table 5. Quantum Theory of Atoms-in Molecules (QTAIM) parameters, the electron density ρ, Laplacian of electron density $\nabla^2\rho(r_c)$, and energy density $E_{\rho(r_c)}$ in au, at the bond critical points (3,−1) at the TSs associated with the formation of new C-C and N-C bonds.

	CP1 (C3-C4)			CP2 (N1-C5)		
	ρ	$\nabla^2\rho(r_c)$	$E_{\rho(r_c)}$	ρ	$\nabla^2\rho(r_c)$	$E_{\rho(r_c)}$
TS1	0.072	0.031	−0.020	0.051	0.091	−0.005
TS2	0.066	0.036	−0.017	0.058	0.091	−0.008
TS3	0.069	0.036	−0.018	0.056	0.092	−0.007
TS4	0.063	0.037	−0.016	0.070	0.091	−0.014
TS5	0.073	0.030	−0.021	0.062	0.092	−0.010
TS6	0.073	0.031	−0.020	0.064	0.091	−0.011

The positive Laplacian of electron density, $\nabla^2\rho(r_c)$ at CP1 and CP2 suggest that the covalent interactions are absent at the interatomic reacting centers of the TSs, also evidenced from the low electron density ρ accumulation at the C3-N2 and N1-C5 bonding regions. Thus, the formation of new covalent bonds has not yet started at the TSs, an observation in complete agreement with the optimized TS geometries (Figure 4) and ELF topological study at the TSs (Table 4).

The IGM [27] analysis is employed as a useful tool to identify and characterize weak NCI. The IGM gradient isosurface adopted for the present study is 0.02 a.u represented for **TS1**, **TS2**, **TS5**, and **TS6** in Figure 7. A very large isosurface extended across the region of interaction between C3-C4 and N1-C5 interacting fragments, indicating the existence of NCI, at the TSs. At **TS1** and **TS5**, a large continuous isosurface for steric interaction between the trimethylsilyl group of TSDE **1**, and TSDA **3** fragments and the carbethoxy group of the DFM **4** fragment is visualized, which is decreased considerably in **TS2** and **TS6**, suggesting the decisive role of the steric influence of the bulky trimethylsilyl group on the stereoselectivity of the 32CA reactions.

TS2 and **TS6** show similitude in the isosurfaces for NCI. Therefore, difference in the activation parameters of **TS2** and **TS6** is not the outcome of steric effects or other non-covalent interactions at the TSs. Instead, the lower activation energy of **TS2** is due to increase in GEDT along the 32CA reaction causing reduction of the EC for depopulation of the C-C double bond in DFM **4**, attributed to the increased polarity induced by the strong nucleophilicity of **1** and strong electrophilicity of **4**, as compared to the moderate nucleophilicity of **3** (Table 2).
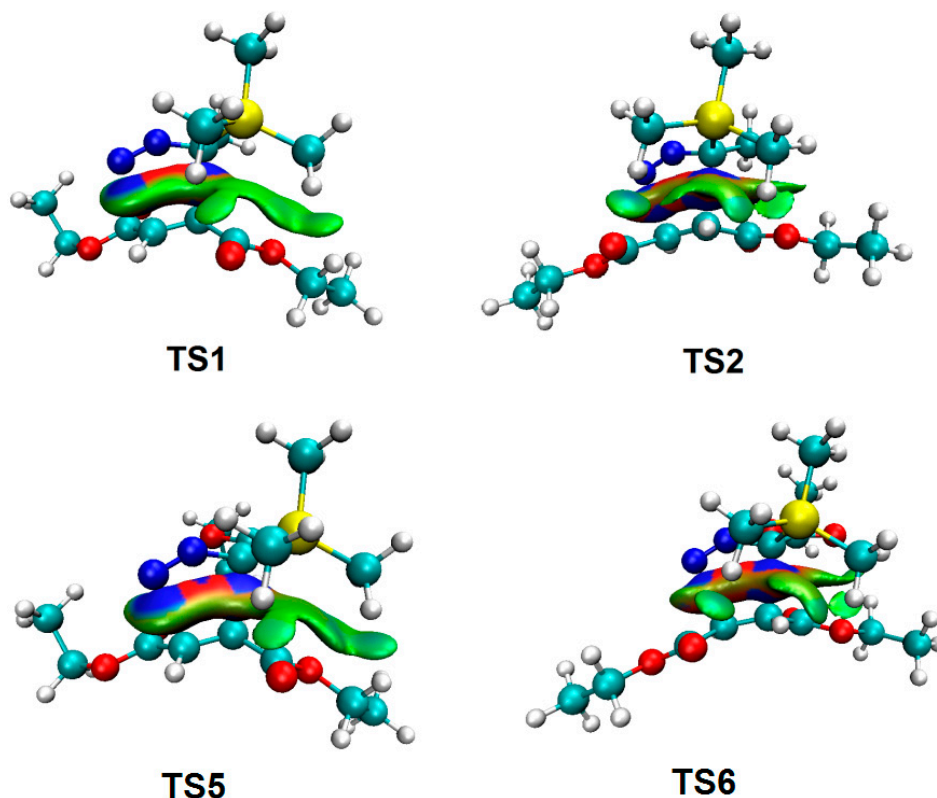
Figure 7. Independent Gradient Model (IGM) analysis of **TS1**, **TS2**, **TS5**, and **TS6** associated with the 32CA reactions of TSDE **1** and TSDA **3** with DFM **4**.

4. Conclusions

32CA reactions of three silyldiazomethane, TSDE **1**, TSDP **2**, and TSDA **3**, with DFM **4** are investigated within the MEDT framework to understand the role of the trimethylsilyl group present in these TACs participating in 32CA reactions.

Topological analysis of the ELF of TSDE **1**, TSDP **2**, and TSDA **3** shows the delocalization of the *pseudoradical* electron density present at the carbon of the simplest diazomethane **11** into the neighboring silicon, changing its structure and reactivity to that of a zwitterionic TAC, thus enabling the participation of these silyldiazoalkanes in *zw*-type 32CA reactions.

The calculated CDFT indices at the GS structures of the reagents show strong nucleophilicity of TSDE **1** and TSDP **2** while TSDA **3** is a moderate nucleophile and DFM **4** is classified as a strong electrophile. Consequently, polar character of these 32CA reactions is comprehended, which is finally confirmed from the calculated GEDT values above 0.20 e at the TSs.

These 32CA reactions follow *one*-step mechanism. The activation enthalpy of the 32CA reaction of TSDE **1** with DFM **4** is lowered by 3.8 and 8.5 kcal·mol^{-1} in CCl$_4$ relative to that of the 32CA reaction of TSDE **2** and TSDE **3** with DFM **4,** respectively, which agrees well with the experimental outcome. These 32CA reactions show negative reaction Gibbs free energies and consequently the exergonic character makes them irreversible. At the preferred stereoisomeric TSs, the trimethylsilyl group of the silyldiazoalkanes is oriented to avoid steric interactions, rendering these 32CA reactions stereoselective.

BET studies for these 32CA reactions indicate that the C3-N2 and C4-C5 bonding regions are depopulated at the initial five phases for the creation of *pseudoradicals* at C3 and C4 carbons and N2 nitrogen lone pair at the TS geometry and finally the generation of new C3-C4 and N1-C5 single bonds takes place at the later phases. 32CA reactions of TSDE **1** show lower EC and higher GEDT values at the IRC points relative to that for the 32CA reactions of TSDE **3**. Thus, the higher GEDT along the 32CA reaction of TSDE **1**, one of the most nucleophilic species of this series, with DFM **4** favors easy rupture of the C-C double bonds, resulting in an acceleration of this reaction compared to the 32CA

reactions of TSDP **2** and TSDA **3** with DFM **4**, in clear agreement with the *zw-type* 32CA reactions. ELF study and topological analysis of the AIM at the TSs indicate that the new C3-C4 and N1-C5 bond formation is not started at the TSs in agreement with the geometrical analysis of the TSs. The steric influence of the trimethylsilyl group on the stereoselectivity is visualized from the IGM analysis.

Finally, it can be concluded that the presence of silicon bonded to the carbon of these silyldiazoalkenes, which enables the delocalization of the electron density of the *pseudoradical* center present in diazomethane **11**, changes the structure and reactivity from that of a *pseudomonoradical* of diazoalkenes to that of a zwitterionic TAC. Thus, polarity plays a decisive role in the feasibility of these 32CA reactions. The increase in GEDT for the 32CA reaction of TSDE **1** with DFM **4** leads to less EC for the rupture of the C4-C5 double bond of DFM **4**, required for the formation of the *pseudoradical* centers needed to form the new C-C and N-C sigma bonds in pyrazolines.

References

1. Presser, A.; Hüfner, A. Trimethylsilyldiazomethane? A Mild and Efficient Reagent for the Methylation of Carboxylic Acids and Alcohols in Natural Products. *Monatshefte Chem. Chem. Mon.* **2004**, *135*, 1015–1022. [CrossRef]

2. Kühnel, E.; Laffan, D.D.P.; Lloyd-Jones, G.C.; del Campo, T.M.; Shepperson, I.R.; Slaughter, J.L. Mechanism of Methyl Esterification of Carboxylic Acids by Trimethylsilyldiazomethane. *Angew. Chem. Int. Ed.* **2007**, *46*, 7075–7078. [CrossRef] [PubMed]

3. Aggarwal, V.K.; Sheldon, C.G.; Macdonald, G.J.; Martin, W.P. A New Method for the Preparation of SilylEnol Ethers from Carbonyl Compounds and (Trimethylsilyl)diazomethane in a Regiospecific and Highly Stereoselective Manner. *J. Am. Chem. Soc.* **2002**, *124*, 10300–10301. [CrossRef] [PubMed]

4. Wu, C.; Bao, Z.; Xu, X.; Wang, J. Metal-free synthesis of gem-silylboronate esters and their Pd(0)-catalyzed cross-coupling with aryliodides. *Org. Biomol. Chem.* **2019**, *17*, 5714–5724. [CrossRef] [PubMed]

5. Sakai, T.; Ito, S.; Furuta, H.; Kawahara, Y.; Mori, Y. Mechanism of the Regio- and Diastereoselective Ring Expansion Reaction Using Trimethylsilyldiazomethane. *Org. Lett.* **2012**, *14*, 4564–4567. [CrossRef]

6. Simovic, D.; Di, M.; Marks, V.; Chatfield, A.D.C.; Rein, K.S. 1,3-Dipolar Cycloadditions of Trimethylsilyldiazomethane Revisited: Steric Demand of the Dipolarophile and the Influence on Product Distribution. *J. Org. Chem.* **2007**, *72*, 650–653. [CrossRef]

7. Brook, A.G.; Jones, P.F. Cycloaddition Reactions of Silyldiazoalkanes. *Can. J. Chem.* **1971**, *49*, 1841–1847. [CrossRef]

8. Hwu, J.R.; Wang, N. Steric influence of the trimethylsilyl group in organic reactions. *Chem. Rev.* **1989**, *89*, 1599–1615. [CrossRef]

9. Padwa, A.; Wannamaker, M.W. Dipolar cycloaddition reaction of diazoalkanes with trimethylsilyl substituted alkynes. Steric control of regiochemistry by the trimethylsilyl group. *Tetrahedron* **1990**, *46*, 1145–1162. [CrossRef]

10. Whitlock, G.A.; Carreira, E. Enantioselective Synthesis ofent-Stellettamide A via a Novel Dipolar Cycloaddition Reaction of (Trimethylsilyl)diazomethane. *J. Org. Chem.* **1997**, *62*, 7916–7917. [CrossRef]

11. Mlostoń, G.; Pipiak, P.; Heimgartner, H. Diradical reaction mechanisms in [3+2]-cycloadditions of hetarylthioketones with alkyl- or trimethylsilyl-substituted diazomethanes. *Beilstein J. Org. Chem.* **2016**, *12*, 716–724. [CrossRef] [PubMed]

12. Mlostoń, G.; Celeda, M.; Jasiński, R.; Heimgartner, H. Experimental and Computational Studies on Stepwise [3+2]-Cycloadditions of Diaryldiazomethanes with Electron-Deficient Dimethyl (E)- and (Z)-2,3-Dicyanobutenedioates. *Eur. J. Org. Chem.* **2018**, *2019*, 422–431. [CrossRef]

13. Bassindale, A.R.; Brook, A.G. Cycloaddition Reactions of Silyldiazoalkanes Involving Rearrangements from Carbon to Nitrogen. *Can. J. Chem.* **1974**, *52*, 3474–3483. [CrossRef]

14. Kohn, W.; Sham, L.J. Self-Consistent Equations Including Exchange and Correlation Effects. *Phys. Rev.* **1965**, *140*, A1133–A1138. [CrossRef]

15. Domingo, L.R. Molecular Electron Density Theory: A Modern View of Reactivity in Organic Chemistry. *Molecules* **2016**, *21*, 1319. [CrossRef]

16. Ríos-Gutiérrez, M.; Domingo, L.R.; Ríos-Gutiérez, M. Unravelling the Mysteries of the [3+2] Cycloaddition Reactions. *Eur. J. Org. Chem.* **2018**, *2019*, 267–282. [CrossRef]

17. Domingo, L.R.; Ríos-Gutiérrez, M.; Perez, P. A Molecular Electron Density Theory Study of the Reactivity and Selectivities in [3+2] Cycloaddition Reactions of C,N-DialkylNitrones with Ethylene Derivatives. *J. Org. Chem.* **2018**, *83*, 2182–2197. [CrossRef]

18. Domingo, L.R.; Acharjee, N. [3+2] Cycloaddition Reaction of C-Phenyl-N-methyl Nitrone to Acyclic-Olefin-Bearing Electron-Donating Substituent: A Molecular Electron Density Theory Study. *Chemistry* **2018**, *3*, 8373–8380. [CrossRef]

19. Domingo, L.R.; Ríos-Gutiérrez, M.; Emamian, S. Understanding the domino reaction between 1-diazopropan-2-one and 1,1-dinitroethylene. A molecular electron density theory study of the [3+2] cycloaddition reactions of diazoalkanes with electron-deficient ethylenes. *RSC Adv.* **2017**, *7*, 15586–15595. [CrossRef]

20. Becke, A.D.; Edgecombe, K.E. A simple measure of electron localization in atomic and molecular systems. *J. Chem. Phys.* **1990**, *92*, 5397–5403. [CrossRef]

21. Geerlings, P.; de Proft, F.; Langenaeker, W. Conceptual Density Functional Theory. *Chem. Rev.* **2003**, *103*, 1793–1874. [CrossRef]

22. Domingo, L.R.; Ríos-Gutiérrez, M.; Perez, P. Applications of the Conceptual Density Functional Theory Indices to Organic Chemistry Reactivity. *Molecules* **2016**, *21*, 748. [CrossRef]

23. Domingo, L.R. A new C–C bond formation model based on the quantum chemical topology of electron density. *RSC Adv.* **2014**, *4*, 32415–32428. [CrossRef]

24. Krokidis, X.; Noury, S.; Silvi, B. Characterization of Elementary Chemical Processes by Catastrophe Theory. *J. Phys. Chem. A* **1997**, *101*, 7277–7282. [CrossRef]

25. Bader, R.F.W. *Atoms in Molecules: A Quantum Theory*; Clarendon Press: Oxford, UK, 1994.

26. Bader, R.F.W.; Essén, H. The characterization of atomic interactions. *J. Chem. Phys.* **1984**, *80*, 1943. [CrossRef]

27. Lefebvre, C.; Khartabil, H.; Boisson, J.; Contreras-García, J.; Piquemal, J.-P.; Hénon, E. The Independent Gradient Model: A New Approach for Probing Strong and Weak Interactions in Molecules from Wave Function Calculations. *ChemPhysChem* **2018**, *19*, 724–735. [CrossRef] [PubMed]

28. Zhao, Y.; Truhlar, D.G. Hybrid Meta Density Functional Theory Methods for Thermochemistry, Thermochemical Kinetics, and Noncovalent Interactions: The MPW1B95 and MPWB1K Models and Comparative Assessments for Hydrogen Bonding and van der Waals Interactions. *J. Phys. Chem. A* **2004**, *108*, 6908–6918. [CrossRef]

29. Hehre, W.J.; Radom, L.; Schleyer, P.V.R.; Pople, J. *Ab Initio Molecular Orbital Theory*; Wiley: New York, NY, USA, 1986.

30. Schlegel, H.B. Optimization of equilibrium geometries and transition structures. *J. Comput. Chem.* **1982**, *3*, 214–218. [CrossRef]

31. Fukui, K. Formulation of the reaction coordinate. *J. Phys. Chem.* **1970**, *74*, 4161–4163. [CrossRef]

32. Gonzalez, C.; Schlegel, H.B. Reaction path following in mass-weighted internal coordinates. *J. Phys. Chem.* **1990**, *94*, 5523–5527. [CrossRef]

33. González, C.; Schlegel, H.B. Improved algorithms for reaction path following: Higher-order implicit algorithms. *J. Chem. Phys.* **1991**, *95*, 5853–5860. [CrossRef]

34. Tomasi, J.; Persico, M. Molecular Interactions in Solution: An Overview of Methods Based on Continuous Distributions of the Solvent. *Chem. Rev.* **1994**, *94*, 2027–2094. [CrossRef]

35. Simkin, B.I.A.; Sheikhet, I.I. *Quantum Chemical and Statistical Theory of Solutions: A Computational Approach*; Ellis Horwood: London, UK, 1995.

36. Cossi, M.; Barone, V.; Cammi, R.; Tomasi, J. Ab initio study of solvated molecules: A new implementation of the polarizable continuum model. *Chem. Phys. Lett.* **1996**, *255*, 327–335. [CrossRef]

37. Cancès, E.; Mennucci, B.; Tomasi, J. A new integral equation formalism for the polarizable continuum model: Theoretical background and applications to isotropic and anisotropic dielectrics. *J. Chem. Phys.* **1997**, *107*, 3032–3041. [CrossRef]

38. Barone, V.; Cossi, M.; Tomasi, J. Geometry optimization of molecular structures in solution by the polarizable continuum model. *J. Comput. Chem.* **1998**, *19*, 404–417. [CrossRef]

39. Reed, A.E.; Weinstock, R.B.; Weinhold, F. Natural population analysisa. *J. Chem. Phys.* **1985**, *83*, 735–746. [CrossRef]

40. Reed, A.E.; Curtiss, L.A.; Weinhold, F. Intermolecular interactions from a natural bond orbital, donor-acceptor viewpoint. *Chem. Rev.* **1988**, *88*, 899–926. [CrossRef]

41. Frisch, M.J.; Trucks, G.W.; Schlegel, H.B.; Scuseria, G.E.; Robb, M.A.; Cheeseman, J.R.; Scalmani, G.; Barone, V.; Petersson, G.A.; Nakatsuji, H.; et al. *Gaussian 16*; Gaussian, Inc.: Wallingford, CT, USA, 2016.

42. Lu, T.; Chen, F. Multiwfn: A multifunctional wave function analyzer. *J. Comput. Chem.* **2011**, *33*, 580–592. [CrossRef]

43. Humphrey, W.; Dalke, A.; Schulten, K. VMD: Visual molecular dynamics. *J. Mol. Graph.* **1996**, *14*, 33–38. [CrossRef]

44. Ahrens, J.; Geveci, B.; Law, C. ParaView: An End-User Tool for Large Data Visualization. In *Visualization Handbook*; Elsevier: Amsterdam, The Netherlands, 2005.

45. Ayachit, U. *The ParaView Guide: A Parallel Visualization Application*; Kitware: New York, NY, USA, 2015.

46. Silvi, B.; Savin, A. Classification of chemical bonds based on topological analysis of electron localization functions. *Nature* **1994**, *371*, 683–686. [CrossRef]

47. Domingo, L.R.; Aurell, M.J.; Perez, P.; Contreras, R. Quantitative characterization of the global electrophilicity power of common diene/dienophile pairs in Diels–Alder reactions. *Tetrahedron* **2002**, *58*, 4417–4423. [CrossRef]

48. Jaramillo, P.; Domingo, L.R.; Chamorro, E.; Perez, P. A further exploration of a nucleophilicity index based on the gas-phase ionization potentials. *J. Mol. Struct. THEOCHEM* **2008**, *865*, 68–72. [CrossRef]

49. Parr, R.G.; Yang, W. *Density Functional Theory of Atoms and Molecules*; Oxford University Press: New York, NY, USA, 1989.

50. Parr, R.G.; Szentpály, L.V.; Liu, S. Electrophilicity Index. *J. Am. Chem. Soc.* **1999**, *121*, 1922–1924. [CrossRef]

51. Domingo, L.R.; Chamorro, E.; Perez, P. Understanding the Reactivity of Captodative Ethylenes in Polar Cycloaddition Reactions. A Theoretical Study. *J. Org. Chem.* **2008**, *73*, 4615–4624. [CrossRef] [PubMed]

52. Domingo, L.R.; Ríos-Gutiérrez, M.; Perez, P. How does the global electron density transfer diminish activation energies in polar cycloaddition reactions? A Molecular Electron Density Theory study. *Tetrahedron* **2017**, *73*, 1718–1724. [CrossRef]